Appl Nanosci (2011) 1:19–26
DOI 10.1007/s13204-011-0003-6

ORIGINAL ARTICLE

Fabrication and characterization of electroless Ni–P–ZrO_2 nano-composite coatings

Yongjian Yang · Weiwei Chen · Chungen Zhou · Huibin Xu · Wei Gao

Received: 7 March 2011 / Accepted: 10 March 2011 / Published online: 5 April 2011

Abstract A novel technique has been developed to produce nano-particle oxide reinforced metal coatings. This method is based on electroless deposition process by adding ZrO_2 sol into conventional electroless Ni–P plating bath. Ni–P–ZrO_2 nano-composite coatings have been produced with highly dispersive ZrO_2 nano-particles inside the alloy coating matrix. The as plated nano-composite coating exhibits much increased microhardness up to 1045 HV_{200} and remarkably improved wear resistance. X-ray and electron diffraction patterns show a phase transformation in the Ni matrix of the coating from amorphous to nanocrystalline when ZrO_2 sol is introduced into the coating. By comparison with the plain Ni–P coating and conventional Ni–P–ZrO_2 composite coating incorporated with solid ZrO_2 powders, two mechanisms for the increased mechanical properties are proposed based on nano-particle dispersion strengthening and phase transformation strengthening. The formation mechanism of ZrO_2 nano-particle is also discussed.

Keywords Electroless plating · Ni–P–ZrO_2 nano-composite coatings · ZrO_2 sol · Oxide nano-particle dispersion · Microhardness · Wear resistance

Y. Yang · W. Chen · W. Gao (✉)
Department of Chemicals and Materials Engineering, The University of Auckland, PB 92019, Auckland, New Zealand
e-mail: w.gao@auckland.ac.nz

C. Zhou · H. Xu
School of Materials Science and Engineering, Beijing University of Aeronautics and Astronautics, Beijing 100191, People's Republic of China

Introduction

Electroless plated nickel coatings (EP Ni–P coatings) have found broad applications due to their good properties and convenient process. The property improvement includes high hardness, good wear and corrosion resistance (Balaraju et al. 2003; Hari Krishnan et al. 2006; Peelers et al. 2001). For enhancing their performance, further development has been achieved mainly by two ways (Balaraju et al. 2003; Agarwala et al. 2006; Apachitei et al. 1998; Mallory and Hajdu 2004; Riedel 1991): incorporating hard or soft particles into the Ni–P matrix and heat treatment. In the past few years, various EP nickel-based composite coatings such as three-component Ni–P–Al_2O_3 (Alirezaei et al. 2007), Ni–P–ZrO_2 (Song et al. 2007; Szczygiel et al. 2008), Ni–P–SiC (Apachitei and Duszczyk 2000; Huang et al. 2004), Ni–P–TiO_2 (Novakovic et al. 2006), Ni–P–diamond (Xu et al. 2005), and Ni–P–B_4C (Araghi and Paydar 2010) and four-component Ni–P–ZrO_2–Al_2O_3 (Sharma et al. 2002) and Ni–W–P–ZrO_2 (Szczygiel et al. 2008) have been explored by suspension of solid ceramic particles in the plating solutions. However, incorporating solid particles can only improve the properties (hardness and wear resistance) of the coatings to a limited level due to the agglomeration of nano- or micro-particles with high surface energy. This severely reduces the particle dispersion strengthening effect in the metal matrix according to the Orowan mechanism (Balaraju et al. 2006; Feng et al. 2007; Hou et al. 2006; Zhang and Chen 2006). On the other hand, although heat treatment can improve the hardness and wear resistance of EP Ni–P deposits to certain extent, it has limited applications to certain types coating systems. For instance, on substrates such as aluminum and magnesium alloys, it can cause undesirable deterioration of their mechanical properties (Apachitei and Duszczyk 2000).

Recently, a novel technique combining sol-gel and electroless plating processing has been developed by (Chen and Gao 2009; Chen et al. 2010) to synthesize EP Ni–P–TiO_2 nano-composite coatings with highly dispersed TiO_2 particles. Without any heat treatment, the novel Ni–P–TiO_2 nano-composite coatings obtained much improved microhardness and wear resistance. This technique utilizes sol solution containing the desirable components to form oxide nano-particles in the electroless plating solution, which can be co-deposited with Ni–P alloy to form nanostructured oxide dispersive composite coatings.

Besides TiO_2 sol, there are also other metallic oxide sols such as ZrO_2 and Al_2O_3 sols (Connor et al. 1995; Liang et al. 2009; Shukla et al. 2002) that can be used to make sol-enhanced composite coatings. This work explores the possibility of using ZrO_2 sol to synthesize EP Ni–P–ZrO_2 nano-composite coatings with improved mechanical properties. The formation mechanism of ZrO_2 nano particles is also discussed.

Experimental

The substrate material was the commercial AZ31 Mg alloy sheet with a composition (wt.%) of 2.33%Al, 1.27%Zn, 0.68%Mn, 0.68%Fe and balanced with Mg. Specimen ($15 \times 10 \times 3$ mm^3) pre-treatment is identical to that described in reference (Chen et al. 2010).

Transparent ZrO_2 sol was prepared by two steps detailed elsewhere (Liang et al. 2009). In the first step, 11.3 mL zirconium(IV) *n*-propoxide (70 wt.% solution in 1-propanol) was dissolved in a mixture containing 30.9 mL anhydrous ethanol and 2.8 mL diethanolamine (DEA). The solution was then kept stirring to achieve a complete chelation between $Zr(OPr)_4$ and DEA. In the second step, a mixture of 0.46 mL deionized water and 4.5 mL ethanol solution was mixed with the solution under vigorous stirring to form a fresh sol.

The bath composition and plating parameters in the present study is presented in Table 1. From the beginning of electroless deposition, ZrO_2 sol was simultaneously dripped into the plating bath with a rate of 0.3–0.4 mL/min. At the same time the solution was kept homogeneous by magnetic stirring at a speed of 200 rpm.

For comparison purposes, plain EP Ni–P coatings and solid powder mixing enhanced "conventional" EP Ni–P–ZrO_2 composite coatings were also prepared with the identical bath composition and plating parameters. In the case of conventional electroless Ni–P–ZrO_2 composite deposition, commercial ZrO_2 powder (Aldrich Chemical Company, Inc.) with a grain size smaller than 5 μm was well dispersed (5 g/L) into the plating bath by stirring before deposition. The content of ZrO_2 particles in the composite coatings was obtained in the same way detailed elsewhere (Chen et al. 2010) by the following equation:

$$C = [\text{Weight}(ZrO_2)/\text{Weight}(\text{Coating})] \times 100\% \quad (1)$$

Since ZrO_2 particles do not react with HNO_3, they were extracted by dissolving the metal matrix into HNO_3 solution. An electronic balance with an accuracy of 0.01 mg was used to measure the quantity of oxide.

The surface and cross-section of the coating were investigated with Philips XL30S FSEM. To determine the coating composition, EDX analysis was performed with every specimen. X-ray diffractometer (Bruker D8) with Cu-$K\alpha$ was used to study the phase structure of the coatings. Crystal size was determined using the Debye–Scherrer relation. The morphologies and distribution of the ZrO_2 particles in the composite coatings were also characterized by JEOL JEM-2100F and FEI Tecnai 12 transmission electron microscopes (TEM). Microhardness of the coatings was determined on a Leco M400 microhardness tester with a Vickers diamond indenter under a 200 g load for a holding time of 15 s. Eight measurements were conducted for each sample and the average was used as the hardness value. Wear tests were conducted on a tribometer (Nanovea TRB) with a friction counterpart of a ruby ball of 6 mm in diameter. A load of 7 N and a sliding speed of 50 mm/s were used without lubrication at ambient temperature. The length of the wear track was 10 mm long and the total elapsed time was 100 min.

Results and discussion

Surface and cross-sectional morphologies of coatings

Figure 1 shows the surface morphologies of the plain Ni–P, conventional Ni–P–ZrO_2 composite and sol enhanced

Table 1 Bath composition and electroless plating parameters

Bath constituents and parameters	Quantity	Bath constituents and parameters	Quantity
$NiSO_4 \cdot 6H_2O$	15 g/L	Thiourea	1 mg/L
$NaH_2PO_2 \cdot H_2O$	14 g/L	ZrO_2 sol	120 mL/L
$NaCH_3COO$	13 g/L	Temperature	80 ± 2°C
HF (40%)	12 mL/L	pH value	6.4 ± 0.2
NH_4HF_2	8 g/L	Time	90 min

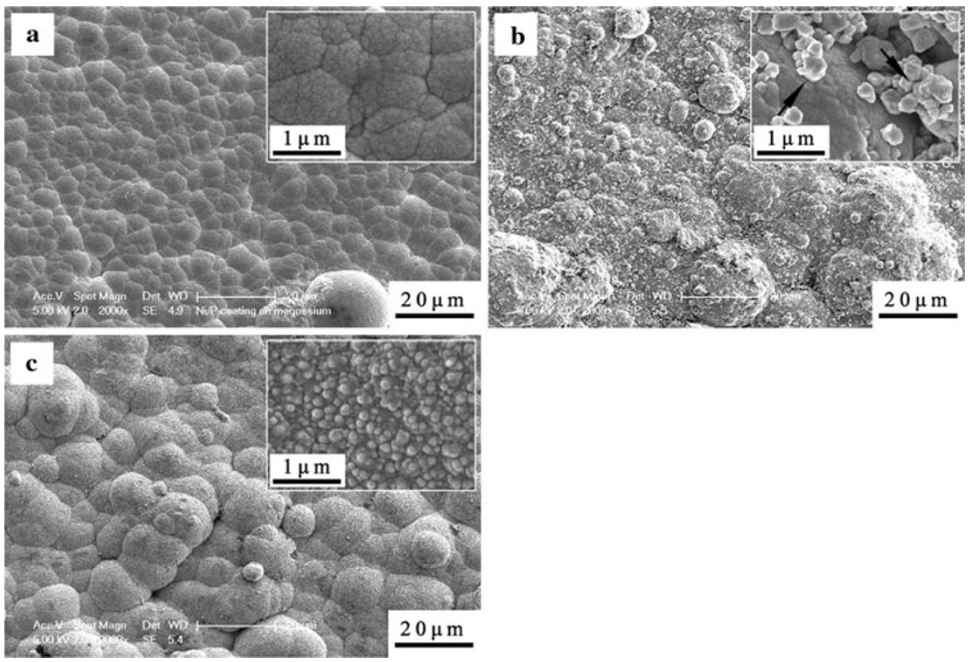

Fig. 1 Surface morphologies of electroless nickel coatings. **a** Plain Ni–P coating, **b** conventional Ni–P–ZrO_2 composite coating, **c** novel Ni–P–ZrO_2 nano-composite coating

novel Ni–P–ZrO_2 composite coatings. Typical spherical nodular structures can be seen on all the three kinds of electroless nickel coatings whereas the two composite coatings have rougher surfaces in comparison with the plain Ni–P. In the inset of Fig. 1b, microsized ZrO_2 particles can be seen clearly on the conventional Ni–P–ZrO_2 composite coating. For the sol processed Ni–P–ZrO_2 composite coating, the inset of Fig. 1c shows a granular morphology throughout the surface, which is also distinct from the smooth surface morphology of Ni–P–TiO_2 composite coatings by others (Chen et al. 2010).

Figure 2 shows the cross-sectional SEM images and qualitative elemental distribution across the plain Ni–P, conventional Ni–P–ZrO_2 composite and novel Ni–P–ZrO_2 composite coatings. All three coatings are compact with uniform thickness of $\sim$20 μm regardless of any surface irregularity, giving a plating rate in the range of 12–14 μm/h. For the conventional Ni–P–ZrO_2 composite coatings, clusters of ZrO_2 particles sized from 200 to 600 nm can be seen in the inset of Fig. 2b1, with a high content of 24.4 ± 0.8 wt%. By contrast, the sol enhanced novel Ni–P–ZrO_2 composite coating exhibits a homogeneous structure without any visible ZrO_2 particles (inset of Fig. 2c1), probably owing to their extremely small size and relatively low content of 4.2 ± 0.5 wt%. The elemental distributions of the three coatings in Fig. 2 show a less quantity but more uniform distribution of Zr in novel Ni–P–ZrO_2 composite coating than in the conventional Ni–P–ZrO_2 composite coating, corresponding to the more dispersive ZrO_2 small particles in the novel Ni–P–ZrO_2 composite coating compared to the micron sized ZrO_2 particles in the conventional Ni–P–ZrO_2 composite coating. At the same time, the lower content of P ($\sim$1.34 wt%) in the novel Ni–P–ZrO_2 composite coating in Fig. 2c2 compared to the other two coatings shown in Fig. 2a2, b2 can be one of the reasons for phase structure transformation in the novel Ni–P–ZrO_2 composite coating which will be detailed in the ensuing section.

TEM observations of coating microstructure and particle morphology

TEM bright field micrographs of the three electroless coatings are shown in Fig. 3. The plain Ni–P coating (Fig. 3a) shows a homogeneous contrast with mixed amorphous and crystalline structures, evidenced by the diffuse rings in the corresponding electron diffraction pattern. For the conventional Ni–P–ZrO_2 composite coating, because the ZrO_2 micron particles are large and have already been confirmed in the above cross-sectional SEM observation, the micrograph (Fig. 3b) only presents the Ni–P matrix structure. As illustrated in the diffraction pattern (inset of Fig. 3b), the microstructure of the conventional Ni–P–ZrO_2 composite coating contains more crystal portion than amorphous phase with sharper rings compared to the plain Ni–P coating. In contrast to both Ni–P and conventional Ni–P–ZrO_2 composite coatings, the novel Ni–P–ZrO_2 composite coating shows a crystal structure containing highly dispersive ZrO_2 nano-particles with the size less than 20 nm as pointed by the arrows (Fig. 3c).

Figure 3d is the TEM micrograph and diffraction pattern of the ZrO_2 particles extracted from the novel Ni–P–ZrO_2

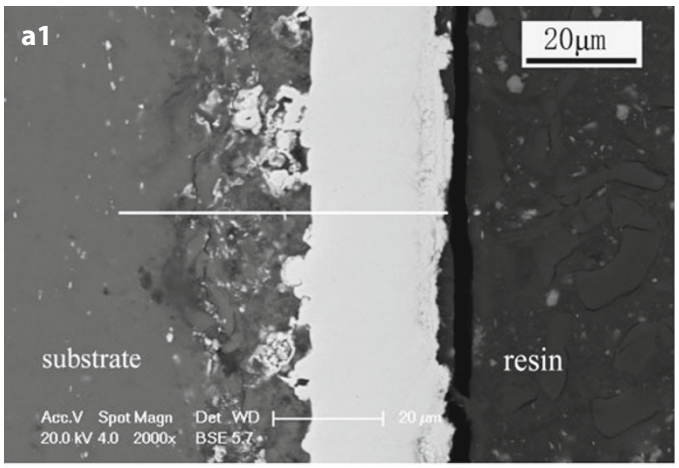

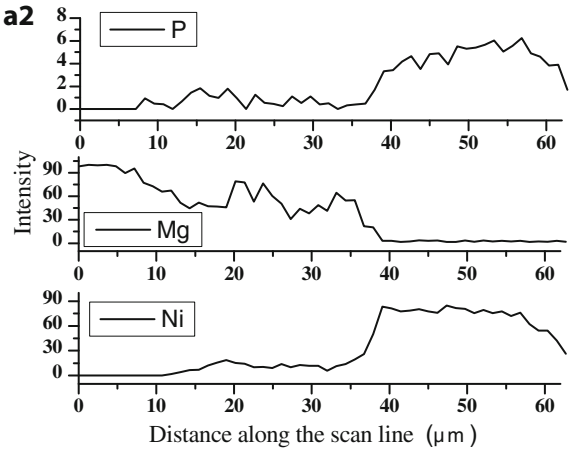

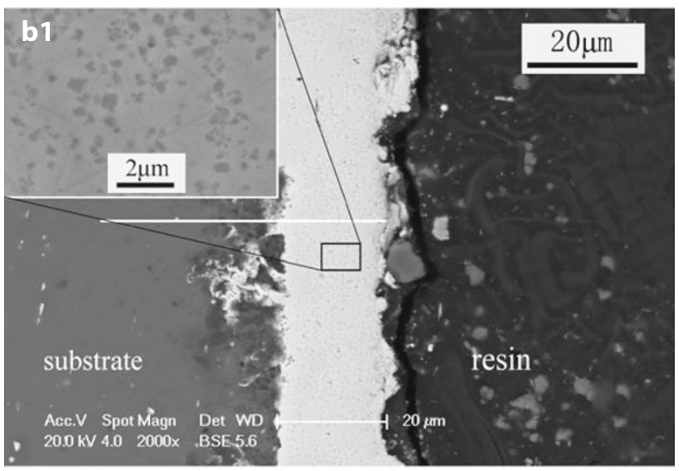

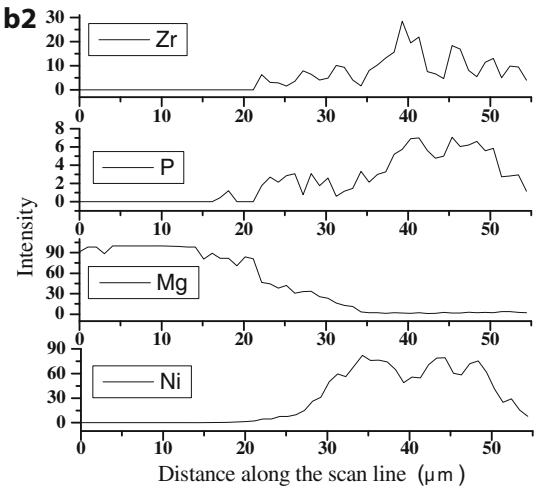

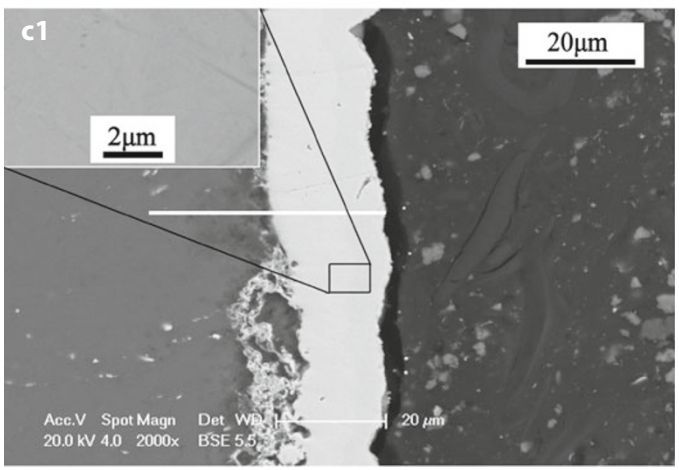

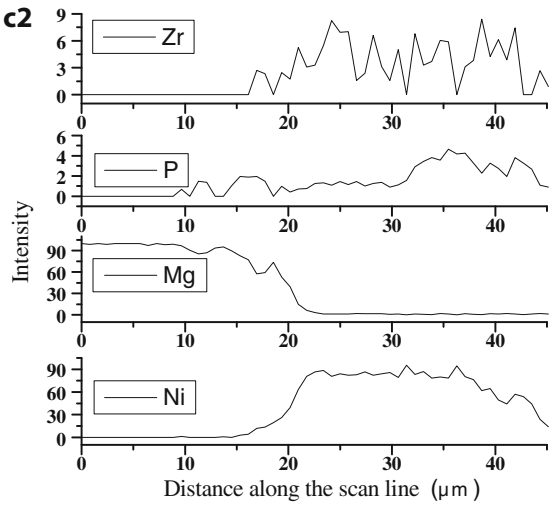

Fig. 2 Cross sections and line scanning analyses results of electroless nickel coatings. **a1**, **a2** Plain Ni–P coating, **b1**, **b2** conventional Ni–P–ZrO_2 composite coating, **c1**, **c2** novel Ni–P–ZrO_2 nano-composite coating

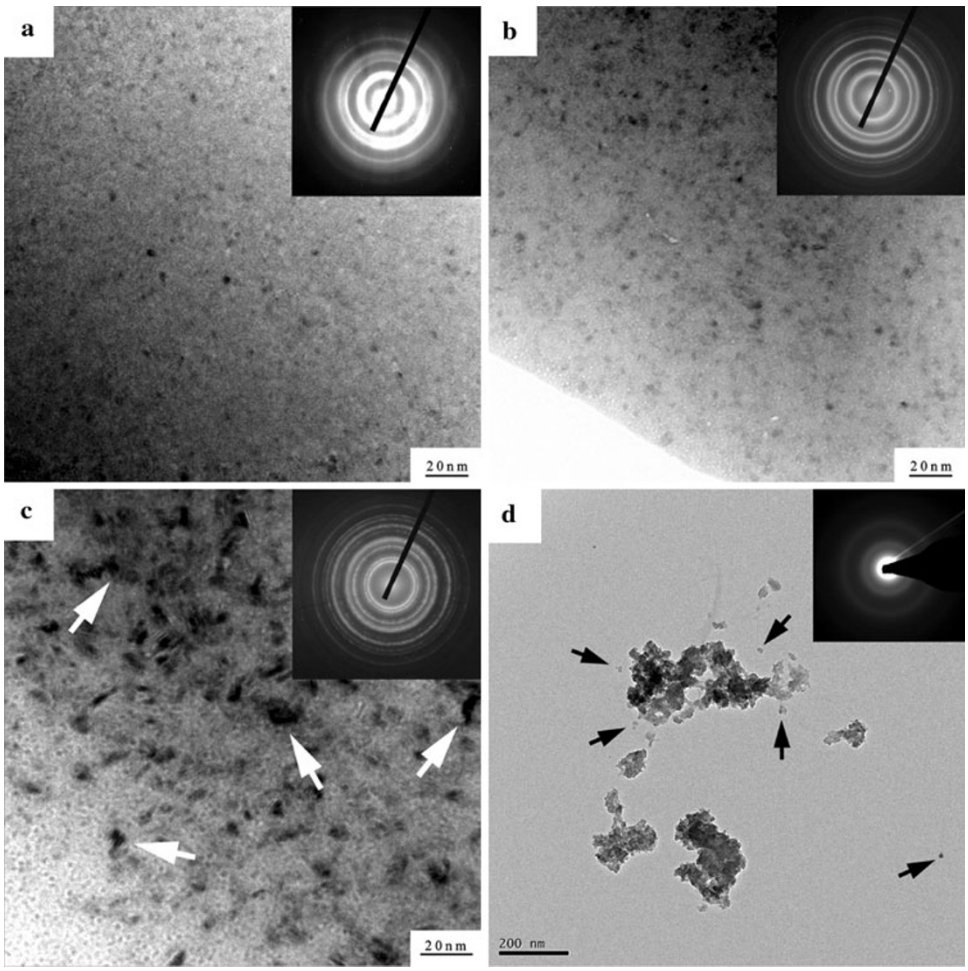

Fig. 3 Typical TEM bright field micrographs and the corresponding SAED patterns showing the microstructures of different coatings. **a** Plain Ni–P coating, **b** conventional Ni–P–ZrO_2 composite coating, **c** novel Ni–P–ZrO_2 nano-composite coating, and **d** the morphology and corresponding electron diffraction pattern of ZrO_2 particles separated from the novel Ni–P–ZrO_2 nano-composite coating

composite coatings. The apparent particle agglomeration shown in Fig. 3d is likely to form after extraction as no such big particles were found in the coatings under SEM and TEM examinations. However, the small particles as arrowed in Fig. 3d represent their original size in the alloy matrix before agglomeration. On the other hand, indication from the diffraction pattern in Fig. 3d does not show a clear crystal structure, which is consistent with the results by electron diffraction pattern of the novel Ni–P–ZrO_2 composite coating, showing no characteristic rings from crystal ZrO_2 particles.

Phase analysis of coatings

Figure 4 is the XRD spectra showing significant differences in phase structure between Ni–P, conventional Ni–P–ZrO_2 composite and the novel Ni–P–ZrO_2 nano-composite coatings. As indicated in the electron diffraction patterns in the former section, both Ni–P and conventional composite coatings are composed of amorphous and crystal phases while the novel Ni–P–ZrO_2 coating is seen fully crystallized with strong diffraction peaks. Since the well-known

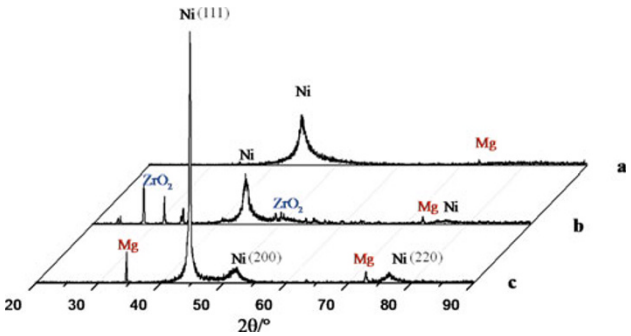

Fig. 4 XRD patterns of electroless nickel coatings. **a** Plain Ni–P coating, **b** conventional Ni–P–ZrO_2 composite coating, **c** novel Ni–P–ZrO_2 nano-composite coating

amorphous structure of the electroless Ni–P coating is attributed to the distortion of crystal lattice of nickel by the phosphorus atoms (Agarwala et al. 2006; Mallory and Hajdu 2004; Sharma et al. 2002), and previous results ("Surface and cross-sectional morphologies of coatings") indicated the lower P content for the novel Ni–P–ZrO_2 coating in contrast with the others, it can be concluded that

Table 2 Microhardness and wear volume loss of plain Ni–P, conventional and novel composite coatings

Type of coating	Microhardness (HV_{200})	Wear volume loss ($\times 10^{-3}$ mm^3)
Plain Ni–P	619 ± 20	25 ± 3
Conventional Ni–P–ZrO_2	759 ± 25	7.3 ± 0.6
Novel Ni–P–ZrO_2	1,045 ± 29	3.7 ± 0.9

the addition of ZrO_2 sol into the electroless Ni–P plating solution decreases the incorporation of P into the coating.

For the conventional Ni–P–ZrO_2 coating, the diffraction peaks from ZrO_2 powders are clearly shown in Fig. 3, consistent with the results from cross-sectional observation which elucidate the existence of crystal ZrO_2 particles in the coating. By contrast, the XRD pattern for novel Ni–P–ZrO_2 nano-composite coating shows no peaks from ZrO_2 particles, again possibly due to the low quantity of the particles (~4.2 wt%) and their amorphous state. Further calculation of grain size by Scherrer method revealed that the crystal sizes for the novel Ni–P–ZrO_2 composite coatings are in the level of ~64 nm, confirming the nano-crystalline structure of the matrix of novel Ni–P–ZrO_2 composite coatings.

Mechanical properties of coatings

Microhardness tests were performed on the plain Ni–P, conventional Ni–P–ZrO_2 and novel Ni–P–ZrO_2 coatings as listed in Table 2. By adding ZrO_2 sol into the electroless Ni–P plating solution to form an optimal nano-composite structure, the microhardness of the novel Ni–P–ZrO_2 composite coating has been increased to a much higher level of 1,045 ± 30 HV_{200} compared to the Ni–P coating of 619 ± 20 HV_{200} and conventional Ni–P–ZrO_2 composite coating of 759 ± 25 HV_{200}.

Figure 5 shows the wear tracks and Table 2 listed the wear volume losses for the three types of coatings. The narrower wear track and shallower plough lines show much improved wear resistance of the novel Ni–P–ZrO_2 composite coatings compared to the plain Ni–P and conventional Ni–P–ZrO_2 composite coatings. While the improved wear resistance of the conventional Ni–P–ZrO_2 composite coating compared to that of plain Ni–P coating can be attributed to the dispersion strengthening and load support function of ZrO_2 particles in the coating (Song et al. 2007), the reasons for the higher microhardness and improved wear resistance of the novel Ni–P–ZrO_2 nano-composite coating possibly come from two perspectives. On one hand, the highly dispersed ZrO_2 nano-particles (<20 nm) can strengthen the Ni–P matrix more effectively than the coarse ZrO_2 particles (200–400 nm) based upon the Orowan mechanism (Hou et al. 2006; Zhang and Chen 2006; Dieter 1976); on the other hand, according to many researchers' results (Apachitei and Duszczyk 2000; Jeong et al. 2002; Van Swygenhoven and Caro 1997), a nano-crystalline structure of the Ni–P-matrix is possessing a higher hardness than an amorphous structure, for which most of explanations are based on a transition from dislocation-controlled deformation to other deformation mechanisms. As illustrated in the XRD and TEM diffraction results, the novel Ni–P–ZrO_2 composite coating show a better crystallized structure than the plain Ni–P and conventional Ni–P–ZrO_2 composite coatings, resulting in a stronger

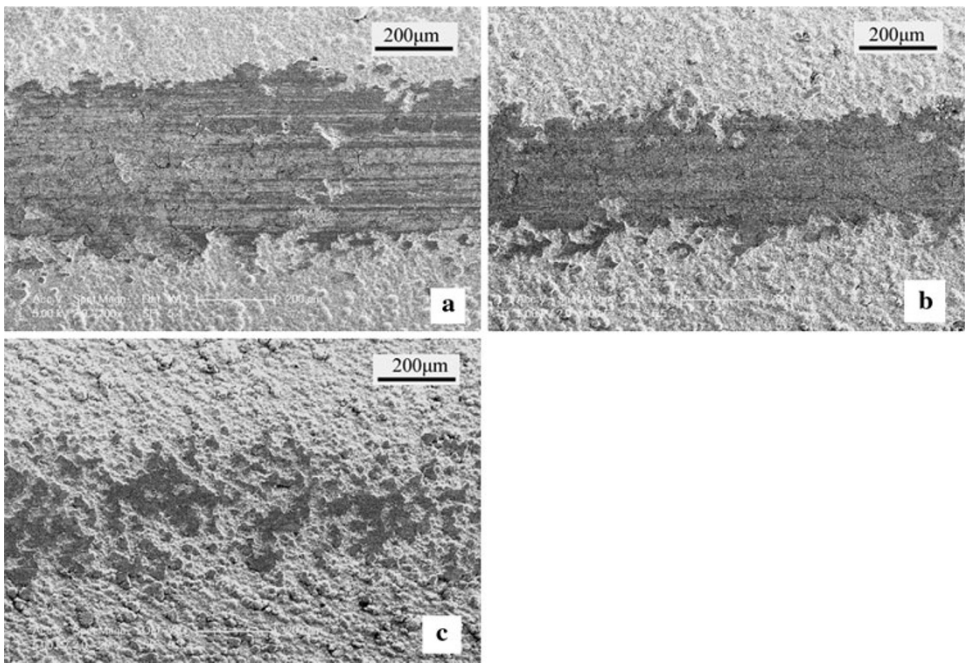

Fig. 5 Micrographs of wear tracks of electroless nickel coatings. **a** Plain Ni–P coating, **b** conventional Ni–P–ZrO_2 composite coating, **c** novel Ni–P–ZrO_2 nano-composite coating

matrix which contributes to the higher hardness and therefore better wear resistance of the nano-composite coatings.

ZrO_2 nano-particle formation mechanism

The formation of the nano-particles during the deposition process can be complicated. A suggested mechanism is presented below. The sol-synthesis method in this study follows the chelating sol-gel route, which produces sols directly based on the hydrolysis-condensation of alkoxides with water (Liang et al. 2009; Qiu et al. 2007). Details about formation mechanism of the metallic oxides particles from the sols have been described in others' works (Gopal et al. 1997; Oleshko et al. 2003; Shukla and Seal 2003; Tang et al. 2003). According to these studies, in the preparation of ZrO_2 sol utilizing neutral ethanol as solvent, condensation process of organic metal macromolecule ions started before completion of hydrolysis, and the formation of ordered structure was hindered, hence the as-synthesized ZrO_2 nano-particles were found to be amorphous as shown in TEM results. The reaction during the preparation can be described as follows:

Hydrolysis:

$$Zr(OC_3H_7)_4 + 4H_2O \rightarrow Zr(OH)_4 + 4C_3H_7OH \quad (2)$$

Condensation:

$$Zr(OH)_4 \rightarrow ZrO_2 + 2H_2O \quad (3)$$

Net reaction:

$$Zr(OC_3H_7)_4 + 2H_2O \rightarrow ZrO_2 + 4C_3H_7OH \quad (4)$$

On the other hand, because the nano-particles in the sol were added dropwise into the plating solution at a controlled speed, it is believed that the particles were well dispersed and some of them were co-deposited into the Ni–P matrix to form the EP nano-composite coatings. This is further supported by TEM observation of the EP Ni–P–ZrO_2 nano-composite coatings, in which particles are seen to uniformly distribute in the Ni–P matrix, with the size smaller than 20 nm.

Conclusion

EP Ni–P–ZrO_2 nano-composite coating has been successfully synthesized via a new process which utilizes metal oxide sol to introduce highly dispersive particles to strengthen the coating. The microhardness for the as-deposited Ni–P–ZrO_2 nano-composite coating was improved to $\sim$1,045 HV_{200} compared to 619 and 759 of the plain Ni–P coating and Ni–P–ZrO_2 coating made by solid particle mixing. Consequently the coating obtains significantly improved wear resistance. The strengthening effects were discussed based on the Orowan dispersion mechanism and properties of different phase structures. The ZrO_2 particle formation mechanism was also discussed in terms of the hydrolysis–condensation reaction. All results from the present study have proved that this new method is an effective way to produce nano-composite coatings with high hardness and wear resistance for promising industrial applications.

Acknowledgments The project is partially supported by a New Zealand Marsden Grant UoA1011 and an Auckland UniServices Grant. The authors would like to thank the technical staff in Department of Chemical and Materials Engineering and Research Centre for Surface and Materials Science for various assistances. Yang also like to thank China Scholarship Council for the International PhD Scholarship, and Mr. Zhaohui Zhou and Lei Liu at the Beijing University of Aeronautics and Astronautics for helping TEM characterization.

References

Agarwala RC, Agarwala V, Sharma R (2006) Electroless Ni-P based nanocoating technology—a review. Synth React Inorg Met Org Nano Met Chem 36:493–515

Alirezaei S, Monirvaghefi SM, Salehi M Saatchi A (2007) Wear behavior of Ni-P and Ni-P-Al2O3 electroless coatings. Wear 262:978–985

Apachitei I, Duszczyk J (2000) Electroless Ni-P composite coatings: the effect of heat treatment on the microhardness of substrate and coating. Surf Coat Technol 132:89–98

Apachitei I, Duszczyk J, Katgerman L, Overkamp PJB (1998) Autocatalytic nickel coatings on aluminium with improved abrasive wear resistance. Scr Mater 38:1347–1353

Araghi A, Paydar MH (2010) Electroless deposition of Ni-P-B4C composite coating on AZ91D magnesium alloy and investigation on its wear and corrosion resistance. Mater Des 31:3095–3099

Balaraju JN, Sankara Narayanan TSN, Seshadri SK et al (2003) Electroless Ni-P composite coatings. J Appl Electrochem 33: 807–816

Balaraju JN, Narayanan TSNS, Seshadri SK (2006) Structure and phase transformation behaviour of electroless Ni-P composite coatings. Mater Res Bull 41:847–860

Chen WW, Gao W (2009) Provisional patent nano-particle ceramic reinforced metal matrix composite coatings, New Zealand

Chen W, Gao W, He Y (2010) A novel electroless plating of Ni-P-TiO_2 nano-composite coatings. Surf Coat Technol 204:2493–2498

Connor PA, Dobson KD, McQuillan AJ (1995) New sol-gel attenuated total reflection infrared spectroscopic method for analysis of adsorption at metal oxide surfaces in aqueous solutions. Chelation of TiO_2, ZrO_2, and Al_2O_3 surfaces by catechol, 8-quinolinol, and acetylacetone. Langmuir 11:4193–4195

Dieter GE (1976) Mechanical metallurgy, 2nd edn. McGraw-Hill, New York, p 774

Feng Q, Li T, Zhang Z, Zhang J, Liu M, Jin J (2007) Preparation of nanostructured Ni/Al_2O_3 composite coatings in high magnetic field. Surf Coat Technol 201:6247–6252

Gopal M, Moberly Chan W, De Jonghe L (1997) Room temperature synthesis of crystalline metal oxides. J Mater Sci 32:6001–6008

Hari Krishnan K, John S, Srinivasan KN, Praveen J, Ganesan M, Kavimani PM (2006) An overall aspect of electroless Ni-P depositions—a review article. Metall Mater Trans A 37:1917–1926

Hou F, Wang W, Guo H (2006) Effect of the dispersibility of ZrO_2 nanoparticles in Ni-ZrO_2 electroplated nanocomposite coatings on the mechanical properties of nanocomposite coatings. Appl Surf Sci 252:3812–3817

Huang X, Wu Y, Qian L (2004) The tribological behavior of electroless Ni-P-SiC (nanometer particles) composite coatings. Plat Surf Finish 91(7):46–48

Jeong DH, Erb U, Aust KT, Palumbo G (2002) The effect of phosphorus content on the structure and wear properties of electrodeposited nanocrystalline Ni-P Alloys. AESF SUR/FIN 2002 Proceedings

Liang L, Xu Y, Wu D, Sun Y (2009) A simple sol-gel route to ZrO_2 films with high optical performances. Mater Chem Phys 114:252–256

Mallory GO, Hajdu JB (2004) American Electroplaters and Surface Finishers Society., Electroless plating: fundamentals and applications, Noyes publications, New York, pp 539, viii

Novakovic J, Vassiliou P, Samara K, Argyropoulos T (2006) Electroless NiP-TiO_2 composite coatings: their production and properties. Surf Coat Technol 201:895–901

Oleshko VP, Howe JM, Shukla S, Seal S (2003) CTEM, HRTEM and FE-AEM investigation of the metastable tetragonal phase stabilization in undoped, sol-gel derived, nanocrystalline zirconia. Microsc Microanal 9:410–411

Peelers P, Hoorn GVD, Daenen T, Kurowski A, Staikov G (2001) Properties of electroless and electroplated Ni-P and its application in microgalvanics. Electrochim Acta 47:161–169

Qiu J, Jin Z, Liu Z, Liu X, Liu G et al (2007) Fabrication of TiO_2 nanotube film by well-aligned ZnO nanorod array film and sol-gel process. Thin Solid Films 515:2897–2902

Riedel W (1991) Electroless nickel plating, ASM International; Finishing Publications Ltd., Metals Park, Ohio Stevenage, England, 320 p

Sharma SB, Agarwala RC, Agarwala V, Satyanarayana KG (2002) Characterization of carbon fabric coated with Ni-P and Ni-P-ZrO_2-Al_2O_3 by electroless technique. J Mater Sci 37:5247–5254

Shukla S, Seal S (2003) Phase stabilization in nanocrystalline zirconia. Rev Adv Mater Sci 5:117–120

Shukla S, Seal S, Vij R, Bandyopadhyay S, Rahman Z (2002) Effect of nanocrystallite morphology on the metastable tetragonal phase stabilization in zirconia. Nano Lett 2:989–993

Song YW, Shan DY, Chen RS, Han EH (2007) Study on electroless Ni-P-ZrO_2 composite coatings on AZ91D magnesium alloys. Surf Eng 23:334–338

Szczygiel B, Turkiewicz A, Serafinczuk J (2008) Surface morphology and structure of Ni-P, Ni-P-ZrO_2, Ni-W-P, Ni-W-P-ZrO_2 coatings deposited by electroless method. Surf Coat Technol 202:1904–1910

Tang Z, Zhang J, Cheng Z, Zhang Z (2003) Synthesis of nanosized rutile TiO_2 powder at low temperature. Mater Chem Phys 77:314–317

Van Swygenhoven H, Caro A (1997) Plastic behavior of nanophase Ni: a molecular dynamics computer simulation. Appl Phys Lett 71:1652–1654

Xu H, Yang Z, Li M-K et al (2005) Synthesis and properties of electroless Ni-P-nanometer diamond composite coatings. Surf Coat Technol 191:161–165

Zhang Z, Chen DL (2006) Consideration of Orowan strengthening effect in particulate-reinforced metal matrix nanocomposites: a model for predicting their yield strength. Scr Mater 54:1321–1326